Generation of high power sub-terahertz radiation from a gyrotron with second harmonic oscillation

Teruo Saito, Naoki Yamada, Shinji Ikeuti, Shinya Ogasawara, Yoshinori Tatematsu et al.

Citation: Phys. Plasmas **19**, 063106 (2012); doi: 10.1063/1.4729316
View online: http://dx.doi.org/10.1063/1.4729316
View Table of Contents: http://pop.aip.org/resource/1/PHPAEN/v19/i6
Published by the American Institute of Physics.

Generation of high power sub-terahertz radiation from a gyrotron with second harmonic oscillation

Teruo Saito,[1] Naoki Yamada,[1] Shinji Ikeuti,[1] Shinya Ogasawara,[2] Yoshinori Tatematsu,[1] Ryosuke Ikeda,[1] Isamu Ogawa,[1] Toshitaka Idehara,[1] Vladimir N. Manuilov,[3] Takashi Shimozuma,[4] Shin Kubo,[4] Masaki Nishiura,[4] Kenji Tanaka,[4] and Kazuo Kawahata[4]
[1]*Research Center for Development of Far-Infrared Region, University of Fukui, 3-9-1 Bunkyo, Fukui 910-8507, Japan*
[2]*Department of Energy Engineering and Science, Nagoya University, Nagoya 464-8463, Japan*
[3]*Nizhny Novgorod State University, Nizhny Novgorod 603600, Russia*
[4]*National Institute for Fusion Science, 322-6 Oroshi-cho, Toki 509-5292, Japan*

(Received 4 March 2012; accepted 2 May 2012; published online 15 June 2012)

New power records of second harmonic gyrotron oscillation have been demonstrated in the sub-THz band. The first step gyrotron of demountable type had succeeded in oscillation with power more than 50 kW at 350 GHz and nearly 40 kW at 390 GHz [T. Notake *et al.*, Phys. Rev. Lett. **103**, 225002 (2009)]. Then, the second step gyrotron of sealed-off type was manufactured. A cavity mode was carefully selected to avoid mode competition with a neighboring fundamental harmonic mode. Matching of the selected mode with the electron gun was also circumspectly considered. The second step gyrotron has attained higher power radiation than the first gyrotron. The maximum single mode power was 62 kW at 388 GHz. Then, the electron gun was modified for use of a different cavity mode with a higher coupling coefficient than that for the 62 kW mode. The new mode proved single mode oscillation power of 83 kW at about 389 GHz. These results are new second-harmonic-oscillation power records for sub-THz gyrotrons. The present study constitutes foundations of development of high power second harmonic sub-THz gyrotron for application to collective Thomson scattering measurement on fusion plasmas, especially on high-density plasmas such as those produced in LHD [N. Ohyabu *et al.*, Phys. Rev. Lett. **97**, 055002 (2006)]. This paper reports the design consideration to realize high power single mode gyrotron oscillation at second harmonic and the examination of oscillation characteristics of the gyrotron. © *2012 American Institute of Physics*. [http://dx.doi.org/10.1063/1.4729316]

I. INTRODUCTION

In recent years, the development of vacuum electronic high power sources in the sub-THz to THz band for application to various fields has been intensified.[1,2] Gyrotrons have attained over one THz oscillations, at both second harmonic (SH) and fundamental harmonic (FH) oscillations.[3,4] Following the successful high frequency oscillation of gyrotrons, application of high frequency gyrotrons has extended to wide fields[5] and many gyrotrons have been developed in the sub-THz frequency band.[6,7] Among many applications of high frequency gyrotrons, sub-THz gyrotrons are very promising to diagnose high-density plasmas. Application of gyrotrons to experiments of scattering from plasmas is very important.[8] Gyrotrons were used for measurement of unstable plasma waves.[9–11] Recently, ion Bernstein wave was measured with a gyrotron.[12] Along with these diagnostics, collective Thomson scattering (CTS) with gyrotrons is one of the most important plasma diagnostics in the current and future magnetic fusion devices.[13] A high power far-infrared laser was applied to CTS in a tokamak.[14] However, a short pulse width inherent to high power far-infrared lasers was a limiting factor for improvement of the signal to noise ratio. Gyrotrons have no inherent limit of the pulse width. High power of the order of 100 kW is necessary as a power source of CTS experiment. Therefore, gyrotrons originally developed for electron heating are currently used in CTS experiments in tokamaks[15] as well as in a stellarator LHD.[16] The frequency range of these gyrotrons is around 100 GHz. Use of a gyrotron with a still lower frequency of 60 GHz has been planned for the future CTS measurement in ITER.[17] However, electromagnetic waves with these frequencies suffer from strong plasma dispersion effects such as refraction and absorption. Moreover, high level background electron cyclotron emission (ECE) is a large noise source. Then, the operation range of experiments is limited.

A sub-THz gyrotron will resolve these problems. Moreover, sub-THz waves satisfy the Salpeter condition $\alpha = 1/k\lambda_D > 1$ over a wide range of the scattering angle for fusion grade plasmas. Here, k is the wave number of the thermal fluctuation of ions and λ_D is the electron Debye length.[8] Then, measurement with the scattering angle at around 90° is possible, which leads to good spatial resolution. For example, when we set the gyrotron frequency at 0.4 THz, the CTS condition is satisfied for a sufficiently large scattering angle over a wide operation range of LHD; the electron density up to several times $10^{20}\,m^{-3}$ and the electron temperature in the range of several keV.[18,19] This frequency is larger than the fifth harmonic electron cyclotron frequency at 2.75 T and hence background ECE can be substantially reduced.

Therefore, 0.4 THz is an appropriate choice. The target power is set to be 100 kW for good signal to noise ratio from calculation of CTS spectrum.[20]

A record of 100 kW at 0.5 THz was reported with FH oscillation.[21] However, a pulse magnet was used in this experiment and oscillation was obtained in single pulses. CW or repetitive pulses are necessary for practical applications. Hence, a DC superconducting magnet should be used. From this point of view, use of SH oscillation is very attractive because the requirement for superconducting magnets is relaxed. SH gyrotrons have been studied for decades.[7,22–24] Recently, development of SH gyrotrons has been intensified in anticipation of new applications.[25–27] However, the powers of these gyrotrons are in the range from tens of watts to kilo watts. The maximum power so far realized in the sub-THz band with SH gyrotron was around 20 kW.[28] Realization of 100 kW-level SH gyrotron oscillation in the sub-THz band is very difficult, because a serious problem of mode competition with neighboring FH modes will appear on this way. Thus, it is a challenge to realize a 100 kW-level sub-THz SH gyrotron. This paper describes results of the development of high power sub-THz gyrotrons with frequencies around 0.4 THz.

Very recently, we have demonstrated greater than 50 kW SH oscillation at 350 GHz and about 40 kW SH oscillation at 390 GHz.[29,30] These powers were realized with careful selection of the oscillation modes and the consideration of the electron optics with consistency with the electron gun design. The gyroton used in this experiment was of demountable type. Then, we have fabricated sealed-off gyrotrons for precise assembly and good vacuum condition. In this paper, we report the significant progress since then achieved with sealed-off gyrotrons.[31] At the first step of this progress, an electron gun with the same electro dynamical design as that of the demountable type gyrotron was used. This electron gun is designed to inject an electron beam into a cavity where the magnetic field strength is as high as 8 T.[32] It generates a laminar electron beam with a high quality for the beam current up to 10 A at the beam voltage of 65 kV. The maximum power obtained with this electron gun was 62 kW. However, the output power saturated with the beam current. Then, the electron gun was modified to change the oscillation mode with a higher coupling coefficient than that of the 62 kW mode. As a result, the output power has attained 83 kW.

High power SH oscillation itself is not sufficient as a high quality power source. Power stability and frequency purity are rather essential. Therefore, the import of the study is confirmation of single mode oscillation. Realization of high power single mode oscillation has been studied for FH gyrotrons.[33–35] High power single mode SH oscillation is much more difficult than FH oscillation, because chance of mode competition with FH modes increases as the beam voltage and the beam current increases.[36] The present study shows a new power record approaching 100 kW as single mode SH oscillation of a gyrotron in the sub-THz band.

Mode competition is, at the same time, a very interesting subject of the gyrotron physics. Experiments[37–39] and theoretical analyses[40–44] have been carried out. The real situation was much more complicated. As shown in Sec. II, there is a chance of mode completion not only with a FH mode but also between SH modes. More than two modes may be excited within the cyclotron resonance band and, moreover, there is a possibility that mode competition between several SH modes and a FH mode. In fact, we have observed many kinds of mode competition, such as simultaneous oscillation of more than two SH modes, excitation of a SH mode as a main mode under oscillation of a FH mode.

The composition of this paper is as follows. Section II describes the design consideration and the electron optics. Emphasis is put on mode selection. Section III is devoted to experimental results obtained with the first electron gun. Experimental results with the modified electron gun are also shown in this section. Section IV discusses the effect of the beam quality on power. The observed mode competition is also discussed from the view point of limiting factors for high power SH oscillation. Finally, conclusions are given in Sec. V.

II. DESIGN CONSIDERATION AND FABRICATION OF GYROTRON

The design task of a high power SH gyrotron in the sub-THz range includes two main points. The first one is reduction of the risk of mode competition. For this to be realized, the oscillation mode should be well isolated from possibly competing modes. In particular, isolation from fundamental modes is very important. The second one is consistency between the design of an electron gun and the electron beam optics for strong coupling with the wave electric field in the cavity. The design of an electron gun that produces a narrow laminar beam with a high quality for a large beam current is difficult task because strong magnetic compression due to the high magnetic field at the cavity makes the electron beam radius very small.[32]

The oscillation frequency is set around 0.4 THz. Figure 1 shows distributions of Bessel prime zeros near candidate modes. The upper and lower numbers correspond to SH and FH resonances, respectively. This region has been carefully chosen by considering the two points mentioned above. There are two candidate modes, $TE_{1,8}$ and $TE_{17,2}$, for which we can expect single mode oscillation because these modes are well isolated from the neighboring FH $TE_{4,3}$ mode. The $TE_{8,5}$

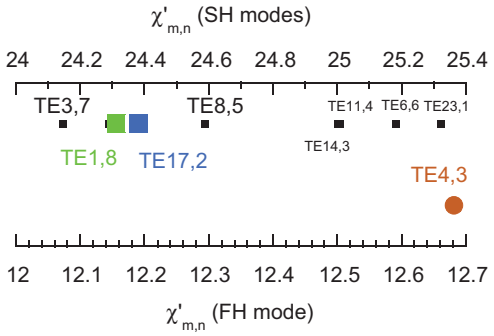

FIG. 1. Distribution of Bessel prime zeros near candidate modes. The upper and lower numbers correspond to SH and FH resonances, respectively. The labels indicate the mode numbers.

mode is not selected because it may be subject to mode competition with the $TE_{4,3}$ mode. We use an electron gun with the same design as that used in the gyrotron of the previous work.[29,30] Therefore, it is also necessary that the electron optics can be made consistent with the electron gun. The necessary magnetic field strength B_c at the cavity is about 8 T for SH oscillation at around 0.4 THz. When this electron gun is used with a magnet field of this strength, the radius R_b of the electron beam at the entrance of the cavity should be set from 1.8 mm to 1.9 mm so that the electron beam has a sufficiently high beam quality, such that, the pitch factor α larger than 1.2, the perpendicular velocity spread is smaller than 10%, and the beam width is smaller than one fourth of the wavelength. Figure 2 shows the cavity profile. The radius and the length of the straight section are 2.99 mm and 12 mm, respectively. These are the same values as those of the demountable type gyrotron.

Then, coupling between the wave electric field and the electron beam is examined. The coupling coefficient is given by the formula[45,46]

$$C_{BF} = \frac{\chi_{m,n}^2 J_{m\pm s}^2(k_{m,n}R_b)}{\pi R_c^2(\chi_{m,n}^2 - m^2)J_m^2(\chi_{m,n})}. \quad (1)$$

Figure 3 plots the radial distributions of the coupling coefficient of the relevant modes. The $TE_{1,8}$ mode has an extreme of C_{BF} at R_b of about 1.8 mm that satisfies the requirement from the electron gun. Then, we first selected the $TE_{1,8}$ mode. The resonance frequency of the cavity calculated with the formula,

$$f_{res} = \frac{c}{2\pi}\sqrt{\left(\frac{\chi_{m,n}}{R_c}\right)^2 + \left(\frac{\pi}{L}\right)^2}, \quad (2)$$

is 388.15 GHz for the $TE_{1,8}$ mode. More precisely, the resonance frequency is calculated from an eigen value equation with a proper boundary condition[47]

$$\frac{d^2V_{m,n}}{dz^2} + \left(\frac{\omega^2}{c^2} - k_{m,n}^2\right)V_{m,n} = 0, \quad (3)$$

where, $V_{m,n}$ is the axial field profile and $k_{m,n} = \chi_{m,n}/R_c$ is the radial wave number. The resonance frequency calculated from Eq. (3) is generally lower than that determined by Eq. (2) because, in open cavities as the present case, the length of axial localization of the RF field is longer than the length L of the straight section of the cavity used in Eq. (2). In fact, the difference is not large for the present case. The resonance frequency calculated from Eq. (3) is 388.10 GHz. This is reasonable because the ratio of the second term to the first term in the square root of Eq. (2) is of the order of 1×10^{-3}. Therefore, we can safely use Eq. (2) for other oscillation modes also.

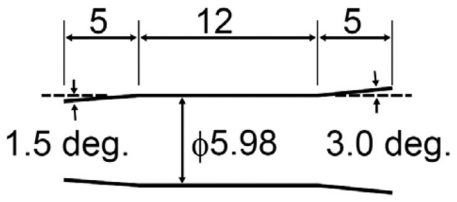

FIG. 2. The cavity profile. The diameter of the straight section is 5.98 mm. That is, the radius is 2.99 mm. The length of the straight section is 12 mm. The electron gun is located to the left and the right side is connected to the vacuum window through an up taper.

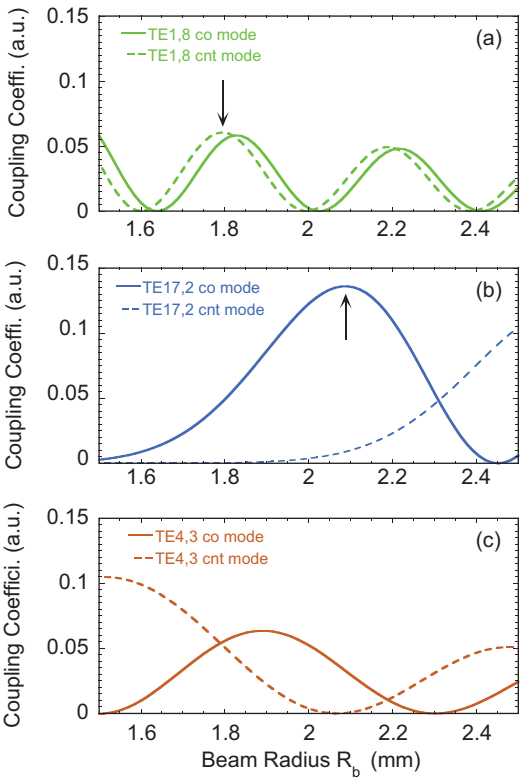

FIG. 3. Radial distribution of coupling coefficient of (a) $TE_{1,8}$, (b) $TE_{17,2}$, and (c) $TE_{4,3}$ modes. The solid line and the dashed line stand for the co-rotating mode and the counter-rotating mode, respectively.

Figure 4 represents start oscillation currents I_S of the relevant modes as functions of B_c.[33,45] The beam voltage V_k and R_b are set at 60 kV and 1.8 mm, respectively. The minimum oscillation currents of about 1 A for the SH modes are low enough. The oscillation region of the $TE_{1,8}$ mode is

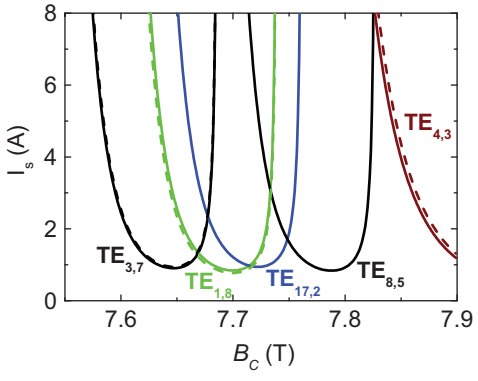

FIG. 4. Start oscillation currents I_S of the relevant modes as functions of the magnetic field strength B_C at the cavity. The solid lines plot I_S for the co-rotating modes and the dashed lines indicate I_S for the counter rotating modes. The beam voltage V_k and the beam radius R_b, and the pitch factor α are set at 60 kV, 1.8 mm, and 1.3, respectively.

sufficiently separated from that of the $TE_{4,3}$ mode for the beam current I_b lower than 10 A. Mode competition calculation with a code described in Ref. 48 predicts that the $TE_{1,8}$ mode is not suppressed by the $TE_{4,3}$ mode at least up to $V_k = 60$ kV and $I_b = 10$ A. The $TE_{8,5}$ mode may suffer from mode competition with the $TE_{4,3}$ mode. There is a region in which I_S for the $TE_{17,2}$ mode and the $TE_{8,5}$ mode is minimum. The mode competition calculation predicts successive turn of oscillation mode with varying B_c. Therefore, for low values of I_b or V_k, a train of single mode oscillation region was expected, which was certainly verified as shown in Sec. III.

However, as I_b or V_k increases, chance of mode competition between neighboring SH modes increases. The condition for competition between two modes of the same cyclotron harmonics is

$$|f_1 - f_2| \leq \Delta f_{CR}, \tag{4}$$

where f_1 and f_2 are frequencies of the two modes.[42] The cyclotron resonance band Δf_{CR} should satisfy the relation $\Delta f_{CR} \leq 1/T$ with $T = L/v_{\parallel}$ being the transit time of an electron through the cavity determined by the cavity length L and the parallel electron velocity $v_{\parallel}$. Figure 4 indicates that the range of B_c of each SH mode is about 0.1 T. This results in $\Delta f_{CR} \sim 3$ GHz. This value is larger than the frequency difference between the frequencies of neighboring SH modes (see Table I), i.e., the relation $|f_1 - f_2| \leq \Delta f_{CR}$ holds. For $V_k = 60$ kV, $\alpha = 1.2$, and $L = 12$ mm, $1/T = v_{\parallel}/L$ is about 5 GHz. Then, the relation $\Delta f_{CR} \leq 1/T$ is also satisfied. Therefore, although the mode competition calculation predicts single mode oscillation of the $TE_{1,8}$ mode in a finite range of B_c, very careful adjustment of the operation condition is necessary.

A sealed off gyrotron with the above design was manufactured. It was mounted on an 8 T superconducting magnet of liquid helium free type. The diameter of the room temperature bore was 100 mm. A triode type electron gun was used. The same dimensions of the electrodes were adopted as used in the previous gyrotron of demountable type. In the following of this paper, the value of R_b is evaluated as $R_b = \sqrt{B_K/B_c} R_K$ using Busch's theorem in paraxial approximation. Here, R_K is the radius of the center of the emission belt on the cathode cone, B_K and B_c are the magnetic field strengths at the cathode and at the entrance of the cavity, respectively. A set of auxiliary coils of ordinary conduction was set at the gun position to adjust B_K. The anode voltage was set at a voltage $V_k R_A/(R_A + R_B)$ with a ratio of the two resisters R_A and R_B inserted between the cathode and the anode and between the anode and the body of the gyrotron, respectively. About 30% of the beam voltage was applied between the cathode and the anode. This ratio was adjusted depending on the operation conditions. The length of the gyrotron was about 1250 mm. The vacuum window was made of a single crystal sapphire disc with the thickness of about 2.5 mm. The c axis was set perpendicularly to the disc surface to avoid double refraction. Operation of the gyrotron was in a pulse mode at the moment. The pulse length was several microsecond and the repetition rate was less than 10 Hz. These were merely limited by a power supply for the beam voltage. The maximum beam voltage V_k was 65 kV. The typical value of the beam current I_b was about 10 A. Since this gyrotron had no internal mode converter, the radiation was extracted as an oscillating mode along the direction of gyrotron axis through the output window.

TABLE I. Measured frequencies of the peaks in Fig. 5 and resonance frequencies of the corresponding SH modes.

Peak No.	Measured frequency (GHz)	Resonance frequency (GHz)	Mode	Δf (GHz)
1	385.11	385.50	$TE_{3,7}$	−0.39
2	387.77	388.15	$TE_{1,8}$	−0.38
3	388.89	389.29	$TE_{17,2}$	−0.40
4	392.15	392.55	$TE_{8,5}$	−0.40

III. EXPERIMENTAL RESULTS

A. Results with the first electron gun

The oscillation intensity was monitored with a pyroelectric detector located at a distance from an open end of a circular waveguide the other end of which is connected to the output window of the gyrotron. A high pass filter (HPF) was inserted in front of the detector to discriminate the FH mode oscillation. It was composed of a bandle of capillaries. The cutoff frequency of the filter is 303 GHz.

An experiment for mode identificaton was first carried out. Figure 5 shows the detector signal as a function of B_c for $V_k = 50$ kV and $I_b = 4$ A. The high pass filter was inserted in front of the detector. Therefore, the signal stands for SH oscillation. The oscillation frequencies were measured with a Fabry-Perot interferometer (FPI) and a heterodyne receiver system with a harmonic mixer. The FPI was always used without the high pass filter to find a FH mode oscillation if it was excited.[38] Table I represents the measured frequencies corresponding to the four peaks in Fig. 5 along with the resonance frequencies f_{res} of the corresponding SH modes calculated with Eq. (2). The measured frequencies agreed with the resonance frequencies very well and hence the oscillation modes were identified as the $TE_{3,7}$ mode, the $TE_{1,8}$ mode,

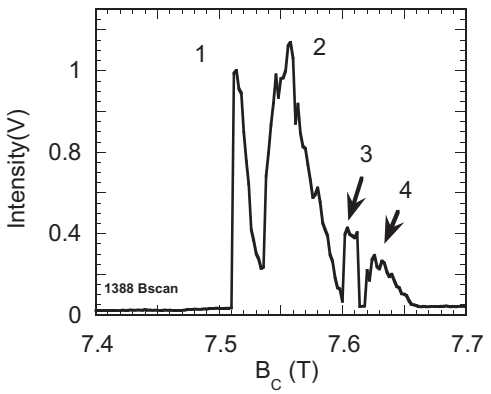

FIG. 5. The pyro electric detector signal as a function of the cavity field B_C for $V_k = 50$ kV and the beam current $I_b = 4$ A. The high pass filter was inserted in front of the detector.

the $TE_{17,2}$ mode, and the $TE_{8,5}$ mode, respectively. There are systematic frequency differences of about 0.4 GHz. A manufacturing error of the cavity radius of about 2.5 μm accounts for these differences. The axial RF profile extending out of the straight section of the cavity may also lower the resonance frequency. However, this effect is very small as examined in Sec. II. Therefore, the manufacturing error of the cavity radius is more likely. The oscillation mode turned successively from the $TE_{3,7}$ mode to the $TE_{8,5}$ mode with increasing B_c. When we set properly the operation condition, the oscillation regions of these modes were separated from each other and simultaneous oscillation of more than two modes did not occur. Therefore, each mode was clearly identified.

When V_k and I_b were increased the gaps between neighboring modes disappeared and hence identification of oscillation mode at a specific value of B_c became difficult. Moreover, chance of mode competition with the FH $TE_{4,3}$ mode increased. Therefore, careful frequency measurement was necessary to identify oscillation mode and to confirm single mode SH oscillation. Oscillation frequency was measured at cardinal values of B_c in the range where oscillation of SH modes was expected. The $TE_{3,7}$ mode, the $TE_{1,8}$ mode, and the $TE_{8,5}$ mode were still identified in this region. However, the $TE_{17,2}$ mode disappeared with increasing V_k and I_b. Figure 6(a) shows the transmission signal of the $TE_{1,8}$ mode through the FPI for $V_k = 60$ kV and $I_b = 8$ A. There was no peak corresponding to the FH $TE_{4,3}$ mode. Therefore, single mode oscillation of the $TE_{1,8}$ mode was confirmed. The frequency width is one of the important factors for applicable to the CTS measurement. Figure 6(b) depicts a typical frequency spectrum of the $TE_{1,8}$ mode measured with the heterodyne receiver. The intermediate frequency (IF) signal from the harmonic mixer was recorded on a fast digital oscilloscope and it was processed with a fast Fourier transform

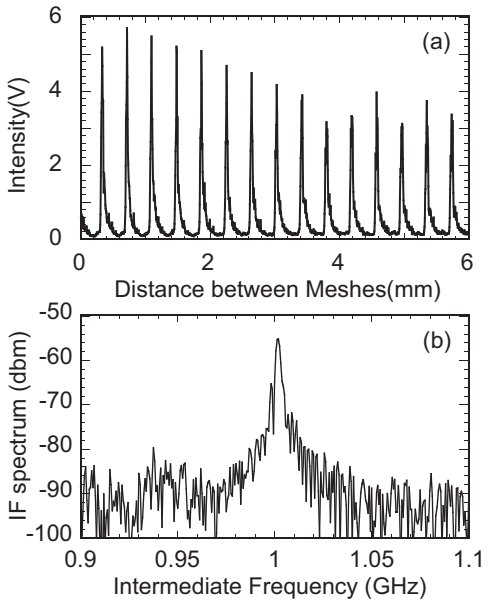

FIG. 6. (a) The transmission signal of the $TE_{1,8}$ mode through the Fabry-Perot interferometer without the high pass filter for $V_k = 60$ kV and $I_b = 8$ A. (b) A typical frequency spectrum of the $TE_{1,8}$ mode measured with the heterodyne receiver. The peak at 1 GHz stands for the $TE_{1,8}$ mode.

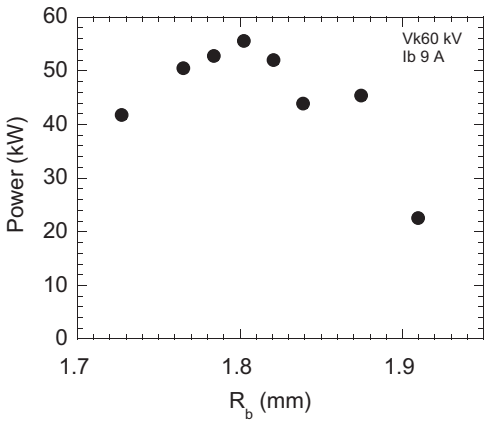

FIG. 7. Power of the $TE_{1,8}$ mode as a function of Rb that was adjusted by changing the auxuliary coil current Igun. The beam voltage and the beam current were fixed at 60 kV and 9 A, respectively.

routine. The peak at 1 GHz stands for the IF frequency corresponding to the $TE_{1,8}$ mode. The 3 dB frequency full width was about 3 MHz, which was almost determined by the pulse width. This width is narrow enough for CTS measurement. Single mode oscillation of the TE3,7 mode was also confirmed. Single mode oscillation of both modes were verified up to $V_k = 60$ kV and $I_b = 10$ A. However, the $TE_{8,5}$ mode often oscillated simultaneously with the FH $TE_{4,3}$ mode.

Among the four SH modes, the $TE_{1,8}$ mode was most powerful for R_b around 1.8 mm in a wide range of V_k and I_b. The output power P of this mode was measured with a water load installed just outside the vacuum window. Figure 7 depicts P as a function of R_b that was adjusted by changing B_k. The values of V_k and I_b were fixed at 60 kV and 9 A, respectively. The output power was maximum at R_b nearly equal to 1.8 mm. This result is consistent with the radial distribution of the coupling coefficient of the $TE_{1,8}$ mode as plotted in Fig. 3. Those for the co-rotating and the counter rotating mode are both maximum at R_b nearly equal to 1.8 mm. This supports validity of the mode identification.

Figure 8 plots P of the $TE_{1,8}$ mode as a function of I_b. The closed circle represents P for $V_k = 60$ kV and the closed squares stand for P for $V_k = 65$ kV. Each data point was obtained with careful adjustment of the operation conditions

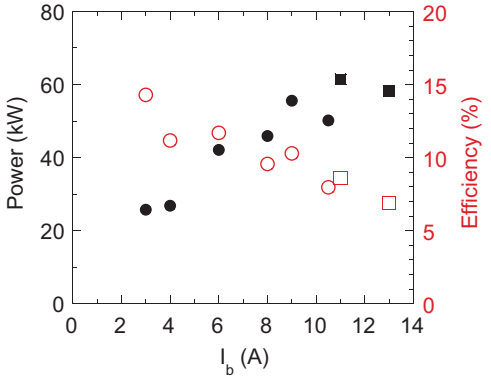

FIG. 8. Beam current dependence of power of the $TE_{1,8}$ mode as a function of I_b. The closed circles represent P for $V_k = 60$ kV and the closed squares stand for P for $V_k = 65$ kV. The open circles represent the efficiency for $V_k = 60$ kV and the open squares indicate that for P for $V_k = 65$ kV.

such as R_b. Single mode oscillation of the $TE_{1,8}$ mode was confirmed for each point by checking the FPI waveform. The output power increased with I_b and attained to 57 kW for $V_k = 60$ kV. However, it slightly decreased at I_b larger than 9 A. This was likely due to deterioration of the beam quality at large I_b. The design of the electron gun was optimized for $V_k = 65$ kV. The operation voltage was limited owing to a problem of the power supply in the early stage of the experiment. Operation voltage was increased to 65 kV after settling this problem. Then, further increase in P was obtained and it reached 62 kW at $I_b = 11$ A. This value was a new power record of SH gyrotron oscillation in the sub-THz band.[31] However, decrease in P at larger I_b still remained. This figure also shows the efficiency with open symbols. It was as high as about 15% for low I_b. However, it decreased with I_b down to about 7% at 13 A. This was likely due to deterioration of the beam quality. Recovery of the efficiency with increase in V_k was limited. Moreover, calculation of the oscillation power with the mode competition code showed difficulty to obtain power more than 100 kW with the $TE_{1,8}$ mode. This was due to rather weak coupling between the electron beam and the wave electric field at an outer radius. The $TE_{1,8}$ mode has many peaks of the coupling coefficient along the radius and the values at each peak decreases with R_b.

B. Modification of the electron gun and consequent results

A way for higher power is use of an oscillation mode that have a larger coupling coefficient. Since the cavity is not changed and the oscillation frequency should keep nealy 400 GHz, it is necessary to search new mode in the vicinity of the $TE_{1,8}$ mode. The $TE_{17,2}$ mode is a promising candidate. However, this mode has a peak coupling at $R_b = 2.09$ mm that is out of the range of R_b allowed from the electron gun design. Therefore, modification of the electron gun design or highly sophisticated operation is necessary to obtain a sufficiently high quality electron beam. Then, a new electron gun with a larger radius of the emission belt than that of the previous one was manufactured. The electron gun was replaced with the new one. Figure 9 shows an example of mode competition calculation for the $TE_{17,2}$ mode for $V_k = 60$ kV, $I_b = 10$ A, $R_b = 2.1$ mm, and $\alpha = 1.2$, respectively. Temporal evolution of the relevant modes at $B_c = 7.6$ T is plotted in Fig. 9(a). This temporal evolution is calculated from nonzero initial values given for each mode under the fixed voltage and current. The $TE_{3,7}$ mode excited first decays rapidly and the $TE_{17,2}$ mode grows subsequently. The $TE_{4,3}$ mode is not excited. Single mode oscillation of the $TE_{17,2}$ mode is established within tens of nanoseconds. This time is much shorter than the pulse width of the experiment. The steady state values of the relevant modes are plotted as functions of B_c in Fig. 9(b). A maximum power higher than 100 kW of the $TE_{17,2}$ mode is expected at B_c slightly lower than 7.6 T. Although the difference from the $TE_{1,8}$ mode is not so large, the $TE_{17,2}$ mode is nearer to the $TE_{4,3}$ mode than the $TE_{1,8}$ mode, and hence mode competition with the $TE_{4,3}$ mode is concerned. However, single mode oscillation of this mode is expected.

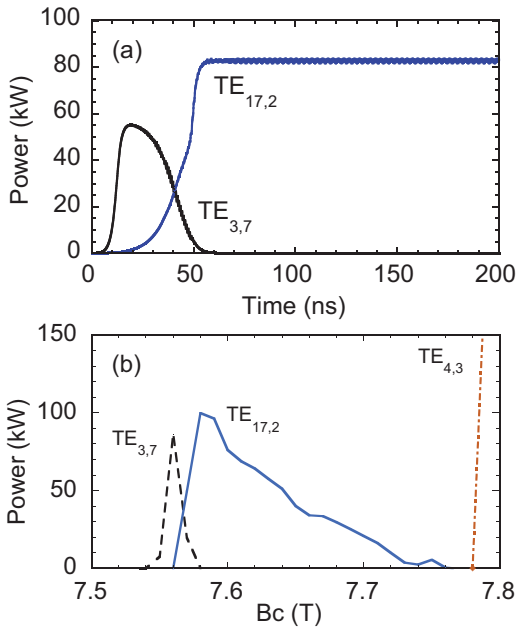

FIG. 9. Mode competition calculation for the $TE_{17,2}$ mode for $V_k = 60$ kV, $I_b = 10$ A, $R_b = 2.1$ mm, and $\alpha = 1.2$, respectively. (a) Time evolution of the $TE_{3,7}$ mode and the $TE_{17,2}$ mode for $B_c = 7.6$ T. (b) Powers of each mode at the steady state are plotted as functions of B_c.

The dependence of the oscillation intensity on the magnetic field B_c at the cavity was examined at first. Figure 10 represents the signal of the pyroelectric detector for $V_k = 60$ kV, $I_b = 10$ A. The dashed line plots the detector signal without the high pass filter and the solid line stands for that with the HPF. The two signals around 7.6 T almost coincide with each other, which means that almost all the signal in this region is attributed to SH oscillation. This supports the calculation shown in Fig. 9 that the SH $TE_{17,2}$ mode oscillates near B_c of 7.6 T without mode competition with the $TE_{4,3}$ mode.

Since the same cavity was used, the frequency of each mode should be the same. Therefore, oscillation modes can be identified from frequency measurement with the heterodyne receiver system. For confirmation of single mode oscillation, however, FPI measurement without the high pass filter is necessary. The FPI measurement would show additional

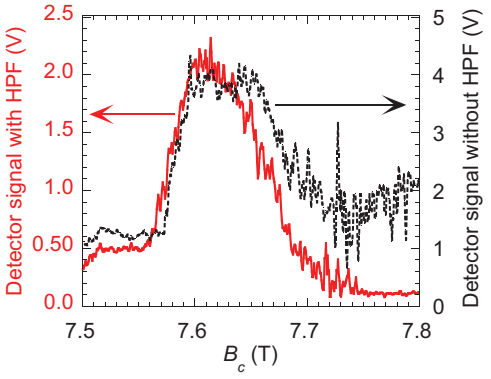

FIG. 10. Dependence of the oscillation intensity on the magnetic field B_c in the cavity. The dashed line plots the detector signal without the high pass filter and the solid line stands for that with the HPF. Small amplitude spikes in the signals were due to the pulse to pulse reproducibility.

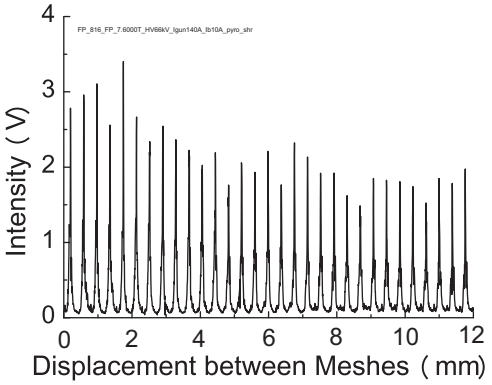

FIG. 11. A transmission signal through the Fabry-Perot interferometer without the high pass filter measured at B = 7.61 T for $V_k = 60$ kV and $I_b = 10$ A.

peaks if there were FH mode oscillation. Figure 11 shows a transmission signal through the FPI measured at $B_c = 7.61$ T for $V_k = 60$ kV and $I_b = 10$ A. The frequency evaluated from the peaks was 388.83 GHz. This was almost equal to the frequency of the $TE_{17,2}$ mode determined above. More accurate frequency measurement with the heterodyne receiver verified this identification. There is no transmission signal corresponding to the $TE_{4,3}$ mode. Therefore, the pulse train stands for the $TE_{17,2}$ mode and single mode oscillation of the $TE_{17,2}$ mode was confirmed.

The output power P was measured in the region of B_c corresponding to the peak of the solid line shown in Fig. 10. It depended on R_b. Figure 12 indicates R_b dependence of P for the case of $V_k = 60$ kV and $I_b = 10$ A. The value of R_b was deduced using Busch's theorem (see Sec. II). The output power strongly depends on R_b and it showed the maximum value at R_b of about 2 mm. In the data shown in Fig. 10, R_b was set not at 2.1 mm but 1.97 mm according to this R_b dependence of P.

The I_b dependence of P is plotted in Fig. 13 for the beam voltage fxed at 60 kV. The cavity field B_c at which the gyrotron deliveres the maximum power varies with I_b. Then, each data point was obtained with fine adjustment of the operation conditions such as B_c and B_k. The output power increased with I_b up to 10 A. The maximum power at 10 A was 83 kW. SH oscillation of the $TE_{17,2}$ mode achieved a

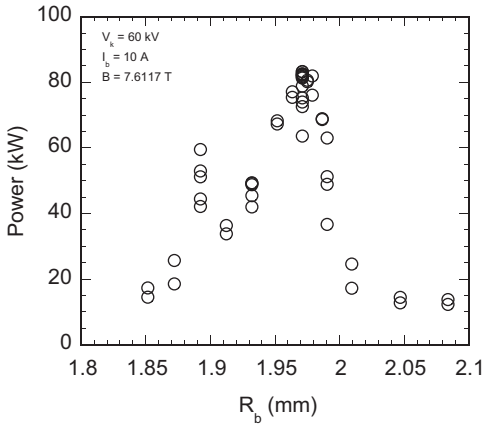

FIG. 12. Beam radius dependence of power for the case of $V_k = 60$ kV and $I_b = 10$ A.

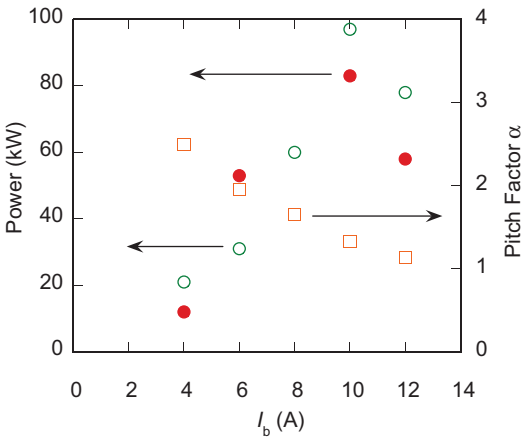

FIG. 13. The I_b dependence of P is plotted with the closed circles. The beam voltage was fxed at 60 kV. The open circles represent calculated value. The open squares stand for the pitch factor evaluated with the code of electron gun design.

still higher power record. The efficiency was 14% for 83 kW. However, power saturation occurred again. The value of P for $I_b = 12$ A was less than 83 kW and the efficiency decreased to lower than 10%. The reason of the power saturation is discussed in Sec. V by comparing with power calculation including variation of the beam quality. Figure 14 compares new power records of SH gyrotron in the sub-THz region with previous achievements. The $TE_{1,8}$ mode recorded 62 kW and the $TE_{17,2}$ mode delivered 83 kW at maximum. We have succeeded in attaining single-mode oscillation of SH gyrotron in the sub-THz band at power levels approaching to 100 kW.

IV. DISCUSSION

As shown in Sec. III, we have demonstrated new power records that are much higher than powers recorded with the demountable gyrotron. However, power saturation occurred again. One of the possible reason is deterioration of the electron beam quality. In particular, decrease in α with I_b has strong influence on power. The open circles in Fig. 13 represent power calculated with the mode competition code. The variation of α with I_b has been evaluated with the elctron

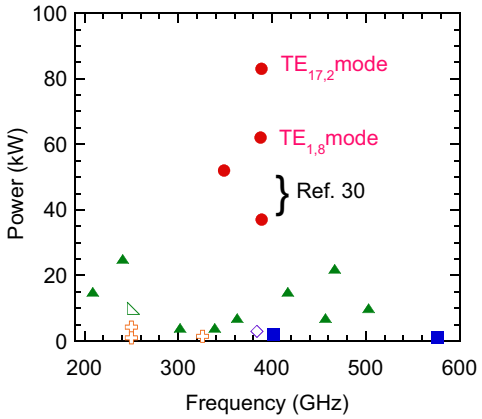

FIG. 14. New power records of SH gyrotron in the sub-THz region with previous achievements. Data other than Ref. 29 were adopted from references cited in Ref. 7.

design code and this effect has been taken into acount in the calculation. Small variations of R_b corresponding to each experimantal data point are used in the calculation. The calculated power increases with I_b and reaches the maximum value almost equal to 100 kW at 10 A. However, it decreases for I_b larger than 10 A as the experimental data did. The velocity spread is also an importan factor of the beam quality and possibly reduces the oscillation efficiency. We have evaluated the relative velocity spread $\delta v_\perp$ with the increase in I_b using the electron gun design code. It increases with I_b and attains about 0.17 for $I_b = 10$ A. It reaches about 0.19 for $I_b = 12$ A. The effect of $\delta v_\perp$ on the oscillation efficiency is examined in Ref. 49. The effect of $\delta v_\perp$ smaller than 0.2 does not play an important role on the efficiency. Therefore, it is considered that a part of the decrease in power is due to the decrease in α.

A latent limiting factor for attaining higher power is mode competition with the FH $TE_{4,3}$ mode. Try to increase in the power of the $TE_{17,2}$ mode by increase in V_k as in the case of the $TE_{1,8}$ mode failed because simultaneous oscillation of the $TE_{4,3}$ mode occurred. In this sense, mode competition blocked the way to higher power. The data shown in Fig. 10 imply potential mode interaction with the $TE_{4,3}$ mode. Namely, contrary to the calculation shown in Fig. 9, oscillation region of the $TE_{4,3}$ mode extended to the region of B_c lower than 7.8 T. A preliminary calculation indicates that the oscillation region of the $TE_{4,3}$ mode extends to the lower field side owing to interaction with SH modes there when R_b is set at the value of 1.97 mm for which the output power was maximum as shown in Fig. 12. This may be an example of nonlinear excitation.[42] For suppression of mode competition with the $TE_{1,8}$ mode, R_b should be slightly smaller than 2 mm. This setting of R_b, on the other hand, increased the possibility of nonlinear interaction with the $TE_{4,3}$ mode because the coupling coefficient of the $TE_{4,3}$ mode increases with decreasing R_b (see Fig. 3). In addition to the nonlinear interaction, Fig. 12 provides an example of competition between the SH modes. The beam radius at which P was maximum was slightly smaller than that for the coupling coefficient (see Fig. 3). Single mode oscillation of the $TE_{17,2}$ mode was confirmed at this R_b as described in Sec. III B. However, the region of single mode region of the $TE_{17,2}$ mode was rather narrow. When R_b was set larger than 2 mm, the $TE_{1,8}$ mode was excited simultaneously and oscillation of the main $TE_{17,2}$ mode became unstable. Simultaneous oscillation of the two modes was also observed for R_b smaller than 1.9 mm. A slight increase in P at $R_b = 1.89$ mm might be a result of mode interaction. However, oscillation was rather unstable. The window of the operation parameters through which single mode SH oscillation was realized became narrow with increasing V_k and I_b.

The combination of interacting modes changed as a function of the operation conditions. In some case, a SH mode was predominant under mode competition with a FH mode. These observations are very interesting from the view point of the gyrotron physics. However, they are too complicated and beyond the scope of the present paper. A detailed study of these phenomena will be published elsewhere.

V. CONCLUSIONS

High power sub-THz second harmonic gyrotrons are under development for application to CTS measurement on fusion plasmas, especially on high-density plasmas such as those produced in LHD. Oscillation modes well separated from FH modes were explored. The consistency between the electron gun and the electron optics was circumspectly considered. Two candidate modes were selected. As the first step, oscillation test with the $TE_{1,8}$ mode was carried out with the electron gun of the same design as the previous demountable type gyrotron. SH oscillations of the $TE_{3,7}$, $TE_{17,2}$, and $TE_{8,5}$ modes as well as the $TE_{1,8}$ mode were identified. The maximun power obtained with the $TE_{1,8}$ mode was 62 kW at 388 GHz, which exceeded the power recorded with the previous gyrotron. Then, a new electron gun was designed for realization of still higher power with the $TE_{17,2}$ mode and oscillation of this mode was tried. As a result, a newer power record of 83 kW at 389 GHz was demonstrated. However, power aturation with the beam current was obsereved. It was shown that the reason of the power saturation was partly due to deterioration of the quality of the electron beam from power calculation that took into account of variation of the pitch factor of the electron beam with the increasing beam current.

Many kinds of mode competition were observed during the present study. Mode competition was a latent limiting factor for higher power and competition between SH modes resulted in decrease in power of the $TE_{17,2}$ mode as shown in Fig. 12. The combination of simultaneously oscillating modes changes as a function of the operation conditions. For example, for V_k greater than 60 kV, we observed simultaneous oscillation of the FH $TE_{4,3}$ mode. In gyrotron physics, it is very interesting to study SH mode oscillation with mode competition with a FH mode. A comprehensive study about mode competition will be published elsewhere.

ACKNOWLEDGMENTS

The authors would like to express their gtatitude to Mr. T. Kanemaki and T. Saito for their technical assistance in the cource of the present study. Stimulated discussions with colleagues in FIR FU are also gratefully acknowledged. The present study was supported by programs of the Grants-in Aid for Scientific Research of Japan Society for the Promotion of Science. It was also supported by the NIFS Collaboration Research programs.

[1]*Modern Microwave and Millimeter-Wave Power Electronics*, edited by R. J. Barker, J. H. Booske, N. C. Luhmann, Jr., and G. S. Nusinovich (IEEE, Piscataway, NJ, 2005).
[2]J. H. Booske, R. J. Dobbs, C. D. Joye, C. L. Kory, G. R. Neil, G.-S. Park, J. Park, and R. J. Temkin, IEEE Trans. Terahertz Sci. Technol. **1**, 54 (2011).
[3]T. Idehara, H. Tsuchiya, O. Watanabe, L. Agusu, and S. Mitsudo, Int. J. Infrared Millim. Waves **27**, 319 (2006).
[4]M. Yu. Glyavin, A. G. Luchinin, and G. Yu. Golubiatnikov, Phys. Rev. Lett. **100**, 015101 (2008).
[5]T. Idehara, T. Saito, I. Ogawa, S. Mitsudo, Y. Tatematsu, and S. Sabchevski, Thin Solid Films **517**, 1503 (2008).
[6]V. Bratman, M. Glyavin, T. Idehara, Y. Karinov, A. Luchinin, V. Manuilov, S. Mitsudo, I. Ogawa, T. Saito, Y. Tatematsu, and V. Zapevalov, IEEE Trans. Plasma Sci. **37**, 36 (2009).

[7]M. Thumm, "State-of-the-art of high power gyro-devices and free electron masers update 2010," KIT Scientific Reports No. 7575, Karlsruhe Institute of Technology.
[8]J. Sheffield, *Plasma Scattering of Electromagnetic Radiation* (Academic, New York, 1975).
[9]N. C. Luhmann and W. A. Peebles, Rev. Sci. Instrum. **55**, 279 (1984).
[10]P. Woskoboinikow, D. R. Cohn, M. Gerver, W. J. Mulligan, R. S.Post, and R. J. Temkin, Rev. Sci. Instrum. **56**, 914 (1985).
[11]I. Ogawa, K. Yoshisue, H. Ibe, T. Idehara, and K. Kawahata, Rev. Sci. Instrum. **66**, 1788 (1994).
[12]S. B. Korsholm, M. Stejner, H. Bindslev, V. Furtula, F. Leipold, F. Meo, P. K. Michelsen, D. Moseev, S. K. Nielsen, M. Salewski, M. de Baar, E. Delabie, M. Kantor, A. Bürger, and TEXTOR Team, Phys. Rev. Lett. **106**, 165004 (2011).
[13]P. Woskoboinikow, D. R. Cohn, and R. J. Temkin, Int. J. Infrared Millim. Waves **4**, 205 (1983).
[14]R. Behn, D. Dicken, J. Hackmann, S. A. Salito, M. R. Siegrist, P. A. Krug, I. Kjelberg, B. Duval, B. Joye, and A. Pochelon, Phys. Rev. Lett. **62**, 2833 (1989).
[15]H. Bindslev, J. A. Hoekzema, J. Egedal, J. A. Fessey, T. P. Hughes, and J. S. Machuzak, Phys. Rev. Lett. **83**, 3206 (1999); H. Bindlev, S. K. Nielsen, L. Porte, J. A. Hoekzema, S. B. Korshlom, F. Meo, P. K. Michelsen, S. Michelsen, J. W. Oosterbeek, E. L. Tsakadze, E. Weserhof, P. Woskov, and TEXTOR team, Phys. Rev. Lett. **97**, 205005 (2006); F. Meo, H. Bindslev, S. B. Korsholm, V. Furtula, F. Leuterer, F. Leipold, P. K. Michelsen, S. K. Nielsen, M. Salewski, J. Stober, D. Wagner, and P. Woskov, Rev. Sci. Instrum. **79**, 10E501 (2008).
[16]S. Kubo, M. Nishiura, K. Tanaka, T. Shimozuma, Y.Yoshimura, H. Igami, H. Takahashi, T. Mutoh, N. Tamura, Y. Tatematsu, T. Saito, T. Notake, S.B. Korsholm, F. Meo, S.K. Nielsen, M. Salewski, and M. Stejner, Rev. Sci. Instrum. **81**, 10D535 (2010); M. Nishiura, S. Kubo, K. Tanaka, N. Tamura, T. Shimozuma, T. Mutoh, K. Kawahata, T. Watari, T. Saito, Y. Tatematsu, and LHD Experiment Group, Plasma Fusion Res. **6**, 2402068 (2011).
[17]F. Meo, H. Bindslev, S. B. Korsholm, E. L. Tsakadze, C. I. Walker, P. Woskov, and G. Vayakis, Rev. Sci. Instrum. **75**, 3585 (2004).
[18]N. Ohyabu, T. Morisaki, S. Masuzaki, R. Sakamoto, M. Kobayashi, J. Miyazawa, M. Shoji, A. Komori, O. Motojima, and LHD Experimental Group, Phys. Rev. Lett. **97**, 055002 (2006).
[19]T. Notake, T. Saito, Y. Tatematsu, S. Kubo, T. Shimozuma, K. Tanaka, M. Nishiura, A. Fujii, L. Agusu, I. Ogawa, and T. Idehara, Rev. Sci. Instrum. **79**, 10E732 (2008).
[20]T. Saito, T. Notake, Y. Tatematsu, A. Fujii, S. Ogasawara, L. Agusu, T. Idehara, S. Kubo, T. Shimozuma, K. Tanaka, M. Nishiura, K. Kawahata, and V. N. Manuilov, J. Phys.: Conf. Ser. **227**, 012013 (2010).
[21]V. A. Flyagin, A. G. Luchinin, and G. S. Nusinovich, Int. J. Infrared Millim. Waves **4**, 629 (1983).
[22]N. I. Zaytsev, T. P. Panktratova, M. I. Petelin, and V. A. Flyagin, Radio Eng. Electron. Phys. **19**, 103 (1974).
[23]G. F. Brand, P. W. Fekete, K. Hong, K. J. Moor, and T. Idehara, Int. J. Electron. **66**, 1099 (1990).
[24]T. Idehara, T. Tatsukawa, I. Ogawa, H. Tanabe, T. Mori, S. Wada, G. F. Brand, and M. H. Brennan, Phys. Fluids B **4**, 267 (1992); T. Idehara, S. Mitsudo, and I. Ogawa, IEEE Trans. Plasma Sci. **32**, 910 (2004).
[25]R. J. Temkin, A. B. Barnes, R. G. Griffin, S. Jawla, I. Mastovsky, E. A. Nanni, M. A. Shapiro, A. C. Torrezan, and P. P. Woskov, in IRMMW-THz 2011, September October 2-7, 2011, Houston, W3A.1. Refrences for many SH gyrotrons developed in Massachusetts Institute of Technology are cited in this paper.
[26]T. Idehara and S. Sabchevski, J. Infrared Millim. Terahertz Waves, **33**, 667 (2012).
[27]V. E. Zapevalov, N. A. Zavol'skiy, O. V. Malygin, M. A. Moiseev, and A. S. Sedov, Radiophys. Quantum Electron. **52**, 878 (2009).
[28]S. Spira-Hakkarainen, K. E. Kreischer, and R. J. Temkin, IEEE Trans. Plasma Sci. **18**, 334 (1990).
[29]T. Notake, T. Saito, Y. Tatematsu, A. Fujii, S. Ogasawara, L. Agusu, V. N. Manuilov, I. Ogawa, and T. Idehara, Plasma Fusion Res. **4**, 011 (2009).
[30]T. Notake T. Saito, Y. Tatematsu, A. Fujii, S. Ogasawara, L. Agusu, I. Ogawa, and T. Idehara, Phys. Rev. Lett. **103**, 225002 (2009).
[31]T. Saito, Y. Tatematsu, N. Yamada, S. Ogasawara, Y. Yamaguchi, T. Idehara, and V. N. Manuilov, in IRMMW–THz 2011, Houston, W3A.5, 3−7 October 2011.
[32]V. N. Manuilov, T. Idehara, T. Saito, L. Agusu, T. Hayashi, and I. Ogawa, Int. J. Infrared Millim. Waves **29**, 1103 (2008).
[33]K. E. Kreischer and R. J. Temkin, Phys. Rev. Lett. **59**, 547 (1987).
[34]D. R. Whaley, M. Q. Tran, A. Alberti, T. M. Tran, T. M. Antonsen, and C. Tran, Phys. Rev. Lett. **75**, 1304 (1995).
[35]K. Sakamoto, A. Kasugai, K. Takahashi, R. Minami, N. Kobayashi, and K. Kajiwara, Nat. Phys. **3**, 411 (2007).
[36]S. H. Kao, C. C. Chu, K. F. Pao, and K. R. Chu, Phys. Rev. Lett. **107**, 135101 (2011).
[37]K. E. Kreischer, R. J. Temkin, H. R. Fetterman, and W. L. Mulligan, IEEE Trans. Microwave Theory Tech. **32**, 481 (1984).
[38]T. Idehara, T. Tatsukawa, I. Ogawa, H. Tanabe, T. Mori, S. Wada, G. F. Brand, and M. H. Brennan, Appl. Phys. Lett. **58**, 1594 (1992); T. Idehara, S. Mitsudo, M. Perayaslavets, Y. Shimizu, and I. Ogawa, Int. J. Infrared Millim. Waves **20**, 1249 (1999).
[39]T. Saito, T. Nakano, S. Mitsudo, I. Ogawa, and T. Idehara, Plasma Fusion Res. **2**, 024 (2007); T. Saito, T. Nakano, H. Hoshizuki, K. Sakai, Y. Tatematsu, S. Mitsudo, I. Ogawa, T. Idehara, and V. E. Zapevalov, Int. J. Infrared Millim. Waves **28**, 1063 (2007).
[40]G. S. Nusinovich, Int. J. Electron. **51**, 457 (1981).
[41]A. W. Fliflet, R. C. Lee, S. H. Gold, W. M. Manheimer, and E. Ott, Phys. Rev. A **43**, 6166 (1991).
[42]G. S. Nusinovich, IEEE Trans. Plasma Sci. **27**, 313 (1999).
[43]P. K. Liu and E. Borie, Int. J. Infrared Millim. Waves **21**, 855 (2000).
[44]G. S. Nusinovich and O. V. Sinitsyn, Phys. Plasmas **14**, 113103 (2007).
[45]M. V. Kertikeyan, E. Borie, and M. K. A. Thumm, *Gyrotrons* (Springer, 2004, Berlin), p. 52.
[46]G. S. Nusinovich, *Introduction to the Physics of Gyrotrons* (The Johns Hopkins University Press, 2004, Baltimore), p. 62.
[47]E. Borie, in *Gyrotron Oscillators, Their Principles and Practice*, edited by C. L. Edgcombe (Taylor & Francis, London 1993), p. 50.
[48]Y. Tatematsu, Y. Yamaguchi, T. Idehara, T. Ozeki, R. Ikeda, T. Kanemaki, I. Ogawa, and T. Saito, J. Infrared Millim. Terahertz Waves **33**, 292 (2012).
[49]N. A. Zavolsky, V. E. Zapevalov, and M. A. Moiseev, Radiophys. Quantum Electron. **49**, 108 (2006).